Effect of Cooling Rate on Phase Transformation Kinetics and Microstructure of Nb–Ti Microalloyed Low Carbon HSLA Steel

Rishabh Bharadwaj[1] [ORCID] · Aditya Sarkar[1] · Bhushan Rakshe[1]

Abstract

Nb–Ti microalloyed low carbon high strength low alloy (HSLA) steels are used to fabricate components, particularly for the automobile and piping applications requiring optimum combination of mechanical properties along with good weldability. These properties depend on the transformed ferrite microstructure and grain size obtained after cooling from hot rolling temperatures which are always well above the austenitizing temperature. Hence, an attempt was made to study the austenite decomposition (phase transformation) kinetics and the accompanying microstructural evolution in Nb–Ti microalloyed steel by subjecting it to austenitization at 1100 °C for 3 min followed by cooling at different rates ranging from 1 to 100 °C/sec in a B*ä*hr DIL 805 A/D dilatometer. The first derivative method was employed to identify critical transformation temperatures from the dilation curves. A modified Johnson–Mehl–Avrami–Kolmogorov (JMAK) analysis (used for non-isothermal conditions) was carried out to find the time exponent (n') values controlling the rate of transformation at different cooling rates. The nature of transformed ferrite was observed to change from polygonal to acicular type, and its grain size was found to decrease with an increase in cooling rate. EBSD analysis also revealed the cooling rate to have a profound effect on the microtexture evolution of the concerned alloy. The "γ" fibre and rotated cube components are replaced by the transformed copper ("α" fibre) components owing to faster transformation and lack of recrystallization of transformed α with increase in cooling rate. Finally, a power law and logarithmic relationship of grain size and microhardness with the applied cooling rate were established.

Keywords Phase transformation · HSLA steel · Kinetics · Ferrite · Dilatometer

Introduction

Low-carbon HSLA steels find many applications in automobile and energy sectors owing to their optimum combination of strength and ductility along with good formability and lean chemistry [1, 2]. Furthermore, these steels possess an added advantage of low carbon equivalent which leads to better weldability characteristics as compared to plain carbon–manganese steels. Adoption of carefully designed thermomechanical processing routes enhances the strength as well as the toughness of these steels with different strengthening mechanisms like grain refinement, solid solution strengthening, dislocation hardening, strain-induced precipitation [3–9] in play. These steels are composed of

ferrite grain matrix with some amount of pearlite depending upon the carbon level. The microalloying elements used in these steels consist of titanium (Ti), niobium (Nb) and vanadium (V). The purpose of adding these microalloying elements is to refine the microstructure, prevent grain growth and enhance the final mechanical properties of the hot-rolled product through precipitation hardening [10]. The stability of precipitates governs the growth behaviour of austenite grains at high temperature [11]. Hence, it is a combination of chemical composition and the thermal cycle (heating as well as cooling) employed during processing that influences the phase transformation start and finish temperatures, kinetics and evolved microstructures. This in turn ultimately affects the final mechanical properties of these steels [12, 13].

One of the means to understand and determine the phase transformation kinetics is to simulate different thermal cycles in a dilatometer [14]. The corresponding dilation curves obtained from such studies are utilized to extract useful information such as phase transformation start and end

✉ Rishabh Bharadwaj
  rishabh2306@gmail.com

1   JSW Steel Limited, Dolvi, India

temperatures, and kinetics. This can be correlated and validated by studying the evolved microstructures. Numerous researchers have studied the phase transformation temperatures and their related kinetics in steels [15–20]. In one such study, Kop et al. [21] developed a model for studying the phase transformation kinetics based on lattice parameters of formed phases as a function of temperature under low cooling rates. Furthermore, a dilatometer test can also be used to generate material's time-temperature-transformation (TTT) and continuous cooling transformation (CCT) diagrams [22]. Apart from a dilatometer, there exist other techniques like differential thermal analysis [23], differential scanning calorimetry [24], synchrotron diffraction [25] and electrical resistivity [26] which can be used to measure phase transformation kinetics. Nonetheless, these techniques are either slow, expensive or difficult to process and sometimes it is unable to mimic the actual industrial conditions.

The modern Compact Strip Production (CSP®) mill in steel industry is equipped with state of art facilities like run-out table (ROT) to control the microstructures of the final hot-rolled product by controlling the water flow rate and hence the cooling rates. It is a well-known fact that the morphology and nature of austenite product phases such as ferrite, pearlite, bainite and martensite are a function of cooling rate which has a direct bearing on mechanical properties of finished product. Hence, it is important to have control over the microstructure in order to achieve desire mechanical properties. There have been various attempts in the past to effectively tailor the product microstructure to achieve optimum combination of mechanical properties by controlling certain characteristics of the final product phase. Smith et al. [27] described the formation of acicular ferrite which induces good combination of strength and toughness to steel. Ghosh et al. [28] in their study showed an enhancement of tensile strength of HSLA-100 steel due to formation of acicular ferrite because of high cooling rate. Furthermore, there also have been attempts to study the textural behaviour of HSLA steels under different thermomechanical treatments [29–33]. One such example is the study conducted by Granados et al. [34] which tracked the evolution of *copper (Cu)*, *brass (Br)*, *transformed Cu* and *transformed Br* components in medium carbon high strength hot-rolled plates cooled at a rapid rate.

Hence, the present study is an attempt to investigate the effect of cooling rate on the phase transformation kinetics, microstructure and microtexture in a low carbon Nb–Ti microalloyed HSLA steel. This is done by performing dilatometric tests on the same to determine its phase

transformation start and end temperatures and evaluate its kinetics. The evolved microstructures have been characterized using optical microscopy, and the corresponding microtexture evolution is studied using electron backscattered diffraction (EBSD) analysis.

Materials and Methods

In the present study, Nb–Ti microalloyed steel was received in the form of 10-mm-thick plate produced through the CSP® route. The chemical composition of the steel under study is given in Table 1. As shown in Fig. 1a, the cylindrical specimens with dimensions of 10 mm length (along rolling direction, RD) $\times$ 4 mm diameter were machined from the centre of the hot-rolled plate. These specimens were subjected to heat treatment tests (thermal cycle shown in Fig. 1b) in a B *ä* hr DIL 805 A/D dilatometer in order to investigate various aspects of austenite to ferrite transformation. The heat treatment cycle consisted of 10 °C/sec ramp up to the austenitizing temperature (T_a) of 1100 °C, followed by a 3 min holding at T_a and then cooling to room temperature with different cooling rates of 1, 10, 30, 50 and 100 °C/s. The solutionizing temperature of 1100°C was selected so as to simulate the reheating of the slab carried out in the equalization furnace prior to hot rolling deformation in hot strip mill. The temperature was controlled and monitored by welding a type-S thermocouple along the circumference at the centre of the sample. The prior austenite grain boundaries (PAGB) were revealed by using the thermal etching method as given in detail in Andres's work [35] to measure the prior austenite grain size at all the test conditions. Furthermore, for analysing the transformed microstructures, the specimen surfaces were prepared by polishing and finishing with 1µm diamond paste followed by etching with 2% Nital solution. The etched specimens were observed under an optical microscope (Olympus DSX 1000). A few heat-treated specimens were selected for electron backscattered diffraction (EBSD) analysis. EBSD scans were conducted on sample surfaces subjected to mechanical polishing followed by electropolishing using the electrolyte consisting of 80% methanol and 20% perchloric acid at 18 V for 18 seconds. The EBSD scans were performed in a FEI NanoSEM attached with EDAX-Velocity EBSD detector. The EBSD scans were carried out on areas of 300 $\times$ 300 µm with a step size of 0.3 µm. All the microstructural observations were carried out and EBSD scans were taken in a specific region on the central plane of the cylindrical specimens as

Table 1 Chemical composition of the Nb–Ti microalloyed HSLA steel

%C	%Mn	%Si	%Nb	%Ti	%Al	%S	%P	%N
0.056	0.761	0.197	0.020	0.027	0.029	0.002	0.004	0.007

Fig. 1 **(a)** Schematic giving the manner of extraction of the cylindrical specimens from the as-received hot-rolled plate and subjected to **(b)** different heat treatment cycles (thermal cycles) in the dilatometer. The specific region observed to study the evolved microstructure post-heat treatment is also shown.
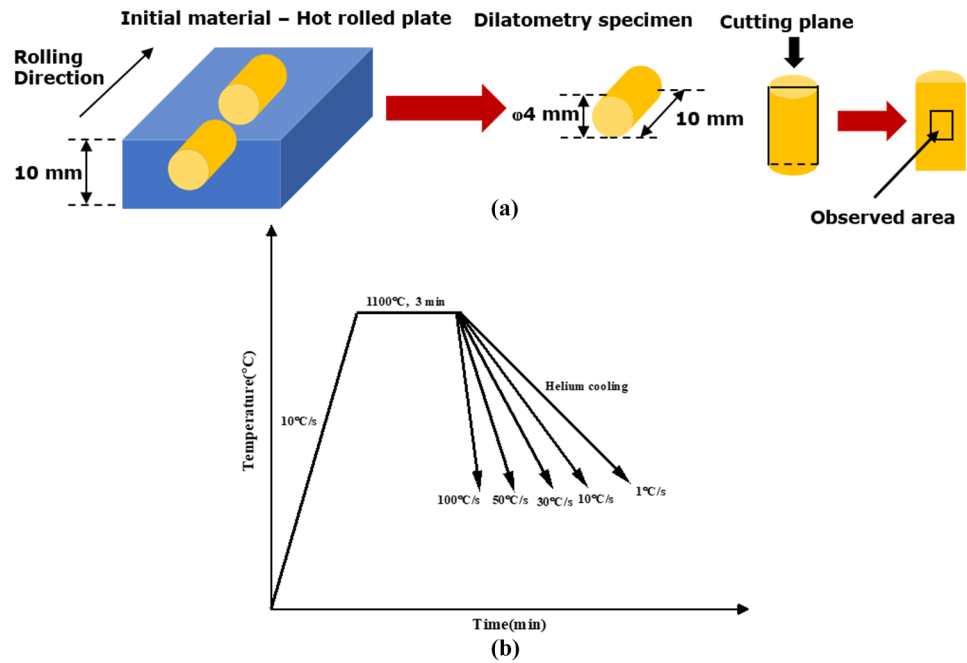
shown in the schematic presented in Fig. 1a. Finally, Vickers microhardness measurements were carried out on all the heat-treated specimens using OMNI TECH S-Auto I. A total of 10 measurements per sample were taken randomly near the centre of the specimen by applying an indentation load of 1 kgf with a dwell time of 10 sec.

Results and Discussion

Phase Transformation Kinetics

The cylindrical specimens were subjected to heat treatments in the dilatometer as per the thermal cycles discussed in the previous section and shown in Fig. 1b. It can be seen that all the specimens were subjected to the same heating rate, austenitizing temperature and soaking time but different cooling rates. This was done in order to ascertain the effect of cooling rate on various aspects of austenite to ferrite transformation of the Nb–Ti microalloyed steel. Hence, the dilatometric curves obtained from the tests during cooling are shown in Fig. 2. In most studies, the line tangent method has been used to identify the austenite to ferrite start temperature (Ar_3) and austenite to ferrite finish temperature Ar_1 temperature. However, determination of Ar_3 and Ar_1 temperature using this method has an element of human error involved in it. Therefore, in the present study, the first derivative method as proposed by Park et al. [36] was used to ascertain the transformation temperature using the dilation data for all cooling rates.

Figure 3 shows the dilation curve and its first derivative $d\varepsilon/dT$ for the sample subjected to the cooling rate of 10 °C/s. The first transformation temperature (Ar_3) was identified as ~ 827 °C. This is the point where the first derivative began to depart from linearity while cooling. Similarly, the Ar_1 was determined at the point where first derivative regains linearity and this was found to be ~ 690 °C. The Ar_1 and Ar_3 determined at all cooling rates using the first derivative method as shown in Fig. 3 are given in Table 2. It can also be observed from Fig. 2 and Table 2 that with an increase in cooling rate, there is a decrease in transformation temperature due to higher levels of undercooling of austenite. The amount of fraction transformed is calculated using Lever rule [37], and the same has been applied in the current work. Figure 4 shows the application of the Lever rule to determine fraction transformed at a particular temperature in the phase transition zone during cooling at a rate of 30 °C/s. Therefore, the fraction of the phase formed is obtained according to the equation:

$$X = \frac{a}{a + b} \tag{1}$$

where a and b are the length of the vertical segments above and below the dilation curve.

Numerous studies have shown that the Lever rule cannot be employed to calculate the fraction transformed in steel when multiple product phases are formed [37–39]. However, the steel used in the present study possesses very low carbon percentage and the product phases formed upon cooling under industrial conditions consist mostly of ferrite with insignificant amounts of pearlite. Hence, the
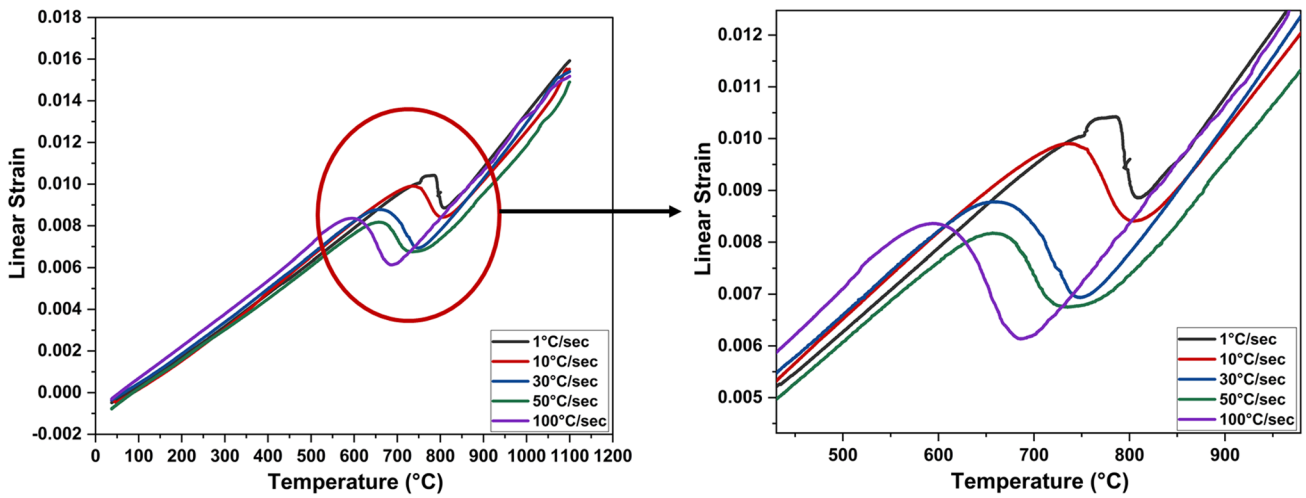
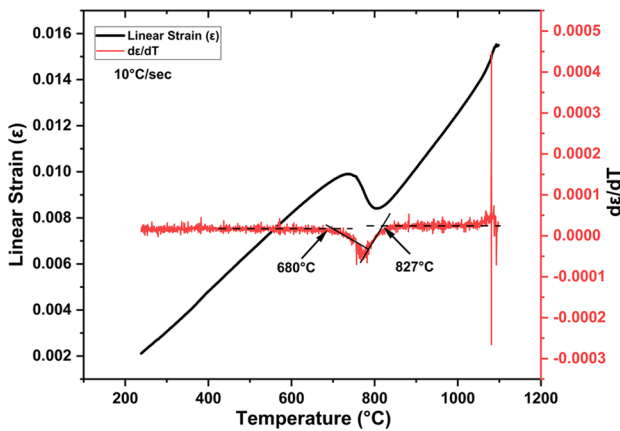**Fig. 2** Dilatometric curves of steel samples at different cooling rates

Fig. 3 Application of the first derivative method to obtain Ar3 and Ar1 temperatures from the studied steel
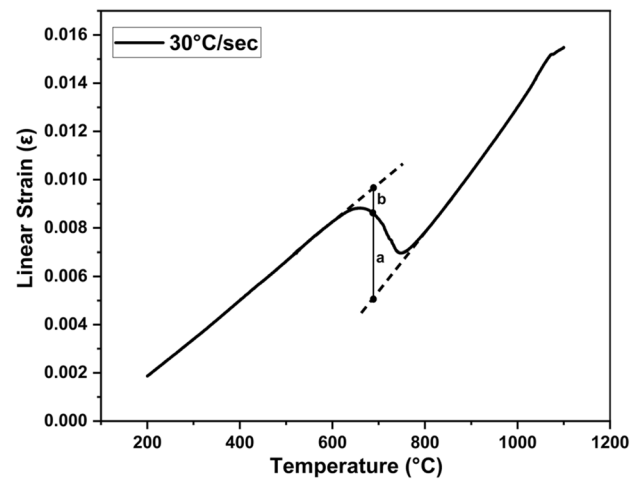
Table 2 Critical transformation temperature obtained from first derivative method

Cooling rate, °C/sec	Ar$_3$ temperature, °C	Ar$_1$ temperature, °C
1	856	762
10	827	680
30	815	597
50	775	614
100	723	548

amounts of ferrite transformed (X) from austenite during cooling from Ar$_1$ to Ar$_1$ a are calculated at all the cooling rates using the Lever rule as shown in Fig. 4b. These fraction transformed values are further utilized to establish

Fig. 4 Lever rule applied to a dilation curve to determine fraction transformed

an equation describing the transformation kinetics for the steel used in the present study.

The most commonly adopted relationship to describe the kinetics of isothermal transformation from austenite to ferrite is the generalized Avrami equation [40].

$$X = 1 - exp(-bt^{n'}) \qquad (2)$$

where X denotes the fraction transformed (calculated using Lever rule in the present study as discussed in the previous section), t is time (given as t $= \Delta T/\varphi$ where $\Delta T = T_{Ar3} - T_i$ (i varies from Ar$_3$ to Ar$_1$) and φ is the cooling rate, b and n' are material constants. Furthermore, this equation has been modified by researchers to also describe the kinetics of non-isothermal γ to α transformation which occurs under
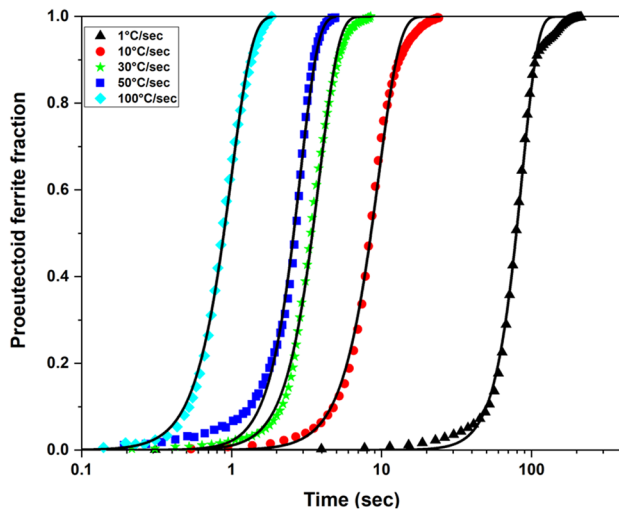
Fig. 5 Plots of ferrite fraction *vs* time subjected to regression analysis to obtain $t_{0.5}$ and n' values at different cooling rates

Table 3 Values of parameter $t_{0.5}$ and exponent n' in expression 2

Cooling rate, °C/sec	$t_{0.5}$	n'
1	79.0	4.11
10	8.48	3.08
30	3.45	3.36
50	2.59	3.63
100	0.86	3.11

continuous cooling conditions. One such modified expression given by Medina et al. [41] is

$$X = 1 - \exp[-ln2(t/t_{0.5})^{n'}] \qquad (3)$$

where $t_{0.5}$ is the time necessary to reach 50% of the ferrite volume fraction.

The Avrami-type equation (Eq 2) employed to describe kinetics under isothermal conditions incorporates both, the nucleation rate as well as the growth rate of ferrite. These have been replaced by a single parameter $t_{0.5}$ in Eq 3 which can be used to better describe the transformation kinetics by studying its variation with different process parameters such as cooling rate, temperature, and composition. [42]. Hence, in the present study, the plots of ferrite fraction vs time as shown in Fig. 5 have been subjected to regression analysis to obtain $t_{0.5}$ and n' values at different cooling rates and are presented in Table 3. Interestingly, the n' values are observed to lie within a narrow range of 3–4 and do not follow a particular trend with respect to cooling rate. This implies that though there is faster initiation of transformation at higher cooling rates, the rate of progression of transformation is almost the same at all cooling rates. In contrast to the

finding made in the present study, researchers have revealed the n' values to increase with increasing cooling rate [43, 44]. This was ascribed to the diffusion-controlled growth of the transformed ferrite being inhibited while interface-controlled growth being favoured at higher cooling rates [45]. This results in the nature of transformed ferrite changing from polygonal to acicular in turn leading to an increase in the n' value with cooling rate. Since no such increase in n' with cooling rate was observed in the present study, microstructural observations are necessitated to ascertain the growth controlling mechanism with respect to cooling rate in the alloy under present study. However, there is a wide variation in the obtained $t_{0.5}$ values as shown in Table 3. Such a variation in pre-exponent ($t_{0.5}$) has been shown to be a result of variation in activation energy for phase transformation with respect to cooling rate [46]. Hence, a single equation describing the phase transformation kinetics encompassing a wide range of cooling rates could not be deduced in the present study using the aforementioned modified JMAK analysis.

Microstructural Evolution

Figure 6a shows the microstructure of the Nb–Ti microalloyed steel obtained in the form of a 10 mm plate with a coiling temperature of 600°C. The microstructure is composed of polygonal ferrite with an average grain size of ~ 10 ± 2 µm. The prior austenite grain boundaries of the as-received material were revealed using thermal etching [35], and the average grain size of the austenite grains was found to be ~ 14 ± 2 µm as shown in Fig. 6b. The microstructural evolution as a function of cooling rate is shown in Fig. 7a–e. It can be observed that at lower cooling rates of 1 and 10 °C/s, microstructure consists of polygonal ferrite with small amounts of pearlite (Fig. 7a–b). With an increase in cooling rate, the amount of pearlite fraction decreases and the morphology of ferrite changes from polygonal ferrite to acicular ferrite (Fig. 7c–e). At the cooling rates of 30 and 50 °C/s, the microstructures are constituted of a mixture of polygonal and acicular ferrite. However, microstructure evolved after cooling at a rate of 100 °C/s is composed majorly of acicular ferrite. The gradual change of ferrite morphology from polygonal to acicular with increase in cooling rate indicates the growth controlling mechanism to change from diffusion controlled to interface controlled as discussed earlier. Figure 8a–c shows the scanning secondary electron images of specimens cooled at rates of 1, 10 and 30 °C/s, respectively. It can be observed that there is gradual degeneration of the lamellar pearlite with increase in cooling rate.

The average grain sizes of the aforementioned microstructures were calculated according to the planimetric method mentioned in the ASTM E112-113 standard. There is a decrease in grain size from ~ 15 to ~4 µm with an

Fig. 6 Optical micrographs of the steel sample in (a) as-received condition (b) Thermal etching to reveal prior-austenite grains
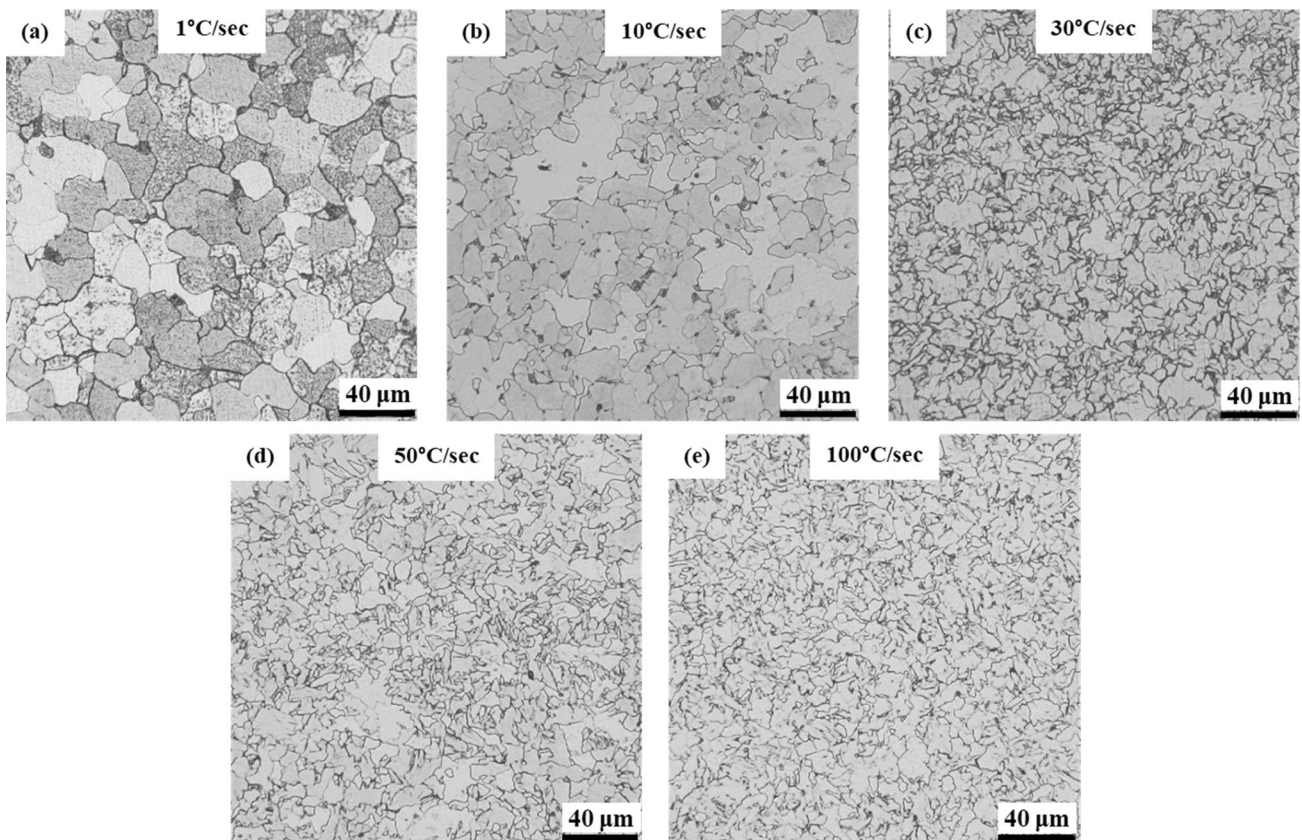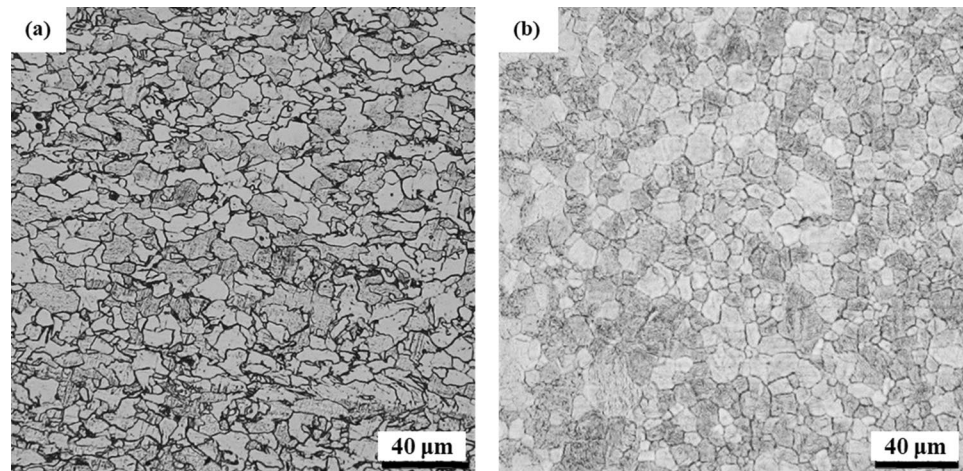

Fig. 7 Optical micrographs of specimens subjected to cooling rate of (a) 1 °C/sec (b) 10 °C/sec (c) 30 °C/sec (d) 50 °C/sec (e) 100 °C/sec

increase in cooling rate from 1 to 100 °C/s. This indicates that higher cooling rates intensified the ferrite nucleation rate thereby restricting the grain growth leading to a fine-grained microstructure with low transformation temperatures products (such as acicular ferrite). Umemoto et al. [47] in their work showed the ferrite grain size relationship with that of the cooling rate and austenite grain size.

$$d_\alpha = A (\varphi)^a (d_\gamma)^b \tag{4}$$

where d_α is the ferrite grain size, A is the pre-exponential constant, φ is the cooling rate, d_γ is the prior austenite grain size, and a and b are fitting constant.
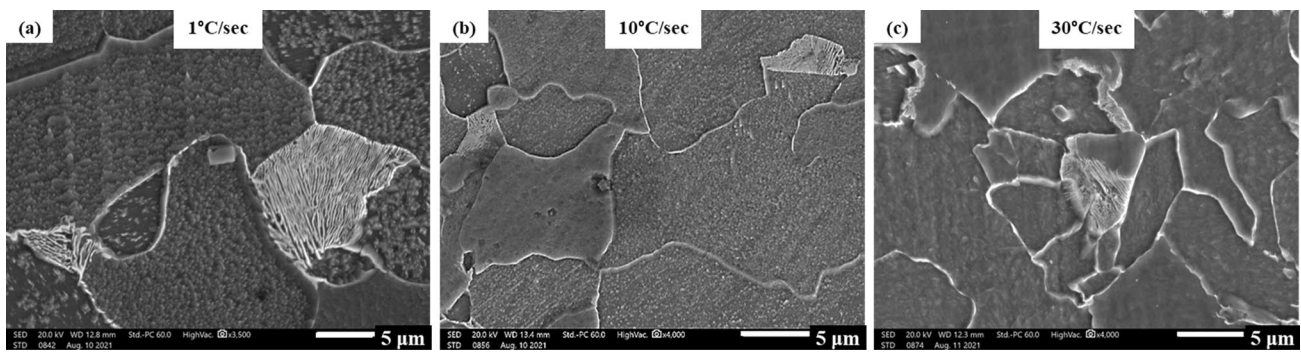
Fig. 8 SEM images of steel samples cooled at a cooling rate of **(a)** 1 °C/sec **(b)** 10 °C/sec **(c)** 30°C/sec showing the transition of morphology of pearlite to degenerated pearlite
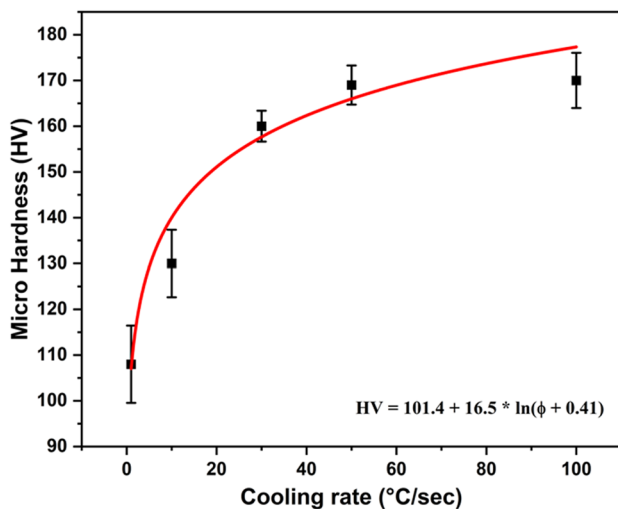

Fig. 9 Variation in microhardness of steel specimens with respect to cooling rate

In the present study, all the specimens were heated to the same austenitizing (holding) temperature and were held there for equal amount of time before being subjected to cooling at different rates. This led to the prior austenite grain size being constant in all the heat-treated specimens. Hence, Eq 4 is modified to obtain a correlation between ferrite grain size and applied cooling rate such that the ferrite grain size exists solely as a function of cooling rate as seen below:

$$d_\alpha = 10.37\,(\varphi)^{-0.14} \tag{5}$$

The microhardness measurements were carried out measured by the Vickers method as per the ASTM standard E384. The change in the morphology of the transformed ferrite and reduction in grain size with increase in cooling rate result in increase in hardness of the steel as shown in Fig. 9. Along with reduction in grain size and change in morphology from polygonal to acicular, another important factor leading to

rise in hardness is inhibition of diffusion of carbon preventing its segregation at higher cooling rates [46].

Furthermore, a relationship was found to exist between the cooling rate and the measured hardness values as given in Eq 6. A similar relationship was reported by Gorni et al. [48] in HSLA-80 and ULCB steels.

$$Microhardness\,(HV) = 101.4 + 16.5 * \ln\,(\varphi + 0.41) \tag{6}$$

EBSD Analysis

Figure 10a and b shows the inverse pole figure (IPF) and boundary map obtained from electron backscattered diffraction (EBSD) analysis of the starting material used in the present study, respectively. Preliminary observation of Fig. 10a suggests <101> (components belonging to the α-fibre) and <100> (cube components) to be the dominant texture components. Furthermore, the ferrite microstructure consists of a mixture of coarse and fine fairly equiaxed polygonal grains with large fraction of high angle boundaries (HABs) as shown from Fig. 10b. In order to further understand and quantify the texture components present in the starting material, the φ_2=45° section of the Euler space (orientation distribution function, ODF) obtained for the same is given in Fig. 10c. The ODF section at φ_2=45° showing the ideal orientations, i.e. "γ" (FCC) rolling texture components and the "α" (BCC) transformation texture components is presented in Fig. 10d for reference [49]. From Fig. 10c, it can be said that the starting material is not heavily textured as the maximum texture intensity is observed to be only ∼ 3.18. Furthermore, upon comparing Fig. 10c and d, it can be observed that even though a combination of "γ" fibre and "α" fibre texture components is present in the starting material; the latter clearly dominates the former. The dominant texture components are closer to {112} <110> (*transformed copper*) and {100} <011> (*rotated cube*) orientations. On the other hand, the minor texture components present in the
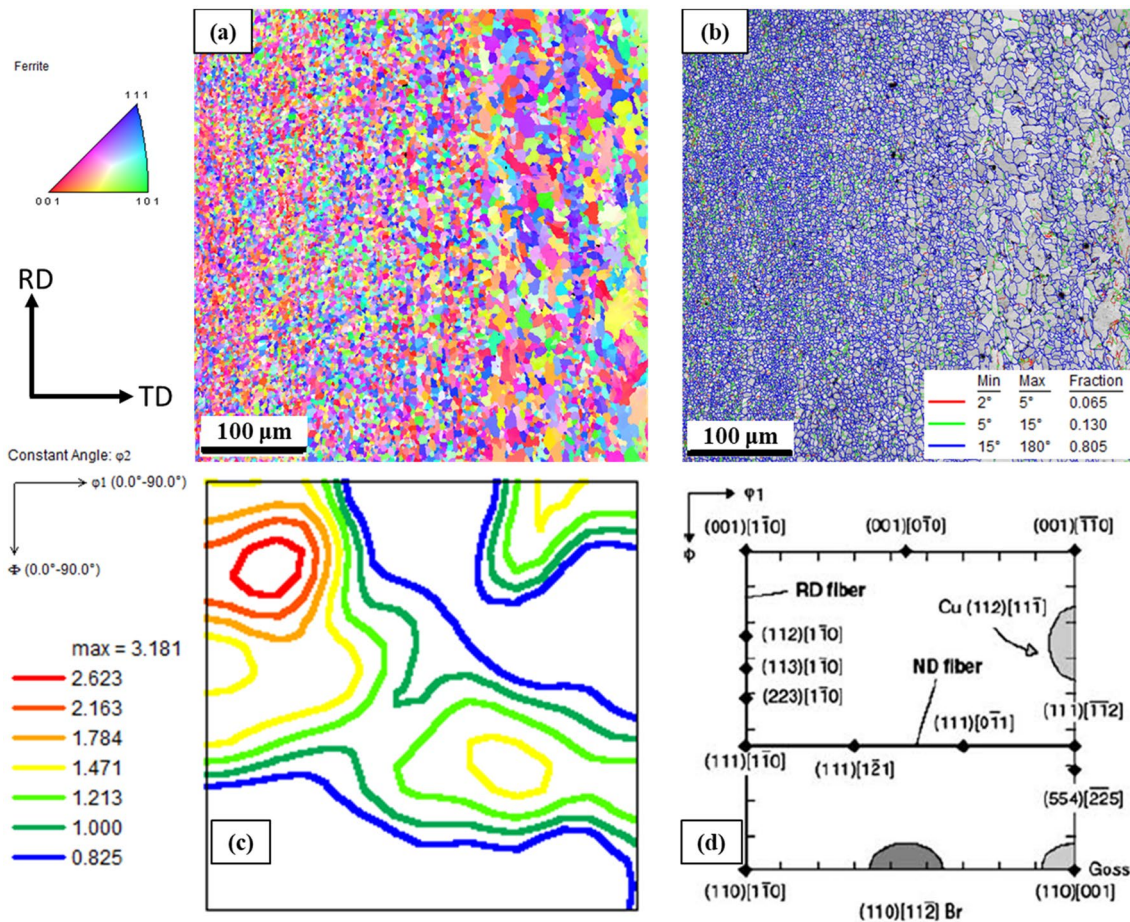
Fig. 10 (**a**) IPF image (**b**) Grain boundary map (**c**) ODF image sectioned at φ_2=45 °C for as-received sample (**d**) Euler space showing the ideal FCC rolling texture components and the transformed BCC components as given in [49]. Reprinted by permission from Springer Nature: Microstructure and Texture in Steels and Other Materials by Arunansu Haldar, Satyam Suwas, and Debashish Bhattacharjee (2009).

starting material are {113} <110>, {223} <110> (both of which are also *transformed copper components*) and {544} <225> (*transformed brass*) [49–51].

Figure 11a–c shows the IPF maps obtained for specimens subjected to different cooling rates of 1, 30 and 100 °C/s, respectively. The corresponding boundary maps are presented in Fig. 11d–f. In the specimen subjected to cooling rate of 1 °C/s, the texture components that appear to be dominant are the <100> (*cube components*). On the other hand, the specimens subjected to cooling rates of 30 and 100 °C/s appear to bear a fairly randomized texture. Furthermore, it can be observed from Fig. 11d–f that there is a decrease in grain size and change in morphology of the transformed ferrite with increasing cooling rate. Additionally, majority of the boundaries in all specimens are characterized as HABs (fraction > 0.7). However, the HAB fraction is observed to decrease and the nature of the microstructures changes from equiaxed and coarse polygonal ferrite to a mixture of fine acicular ferrite and coarse polygonal ferrite with increasing

cooling rate. Similar observations have been extensively reported in the literature available on effect of cooling rate on morphology of transformed products [52].

In order to better understand the effect of cooling rate on the texture evolution of Nb–Ti microalloyed steel, the φ_2=45° sections of the ODFs generated from EBSD analysis of specimens subjected to different cooling rates of 1, 30 and 100 °C/s are shown in Fig. 12a–c, respectively. It can be observed from Fig. 12a that the specimen subjected to cooling rate of 1 °C/s exhibits strong *rotated cube* texture components along with a presence of a weak "γ" fibre. The dominant texture components in the specimen subjected to cooling rate of 30 °C/s are {112} <110>, {113}<110> and {544}<225> in addition to the rotated cube components as shown in Fig. 12b. In specimen cooled at 100 °C/s, the only texture components that are dominant belong to the "α" fibre, viz. {112}<110> and {113}<110>. It can also be seen from Fig. 12a–c that there is a gradual disintegration of the "γ"
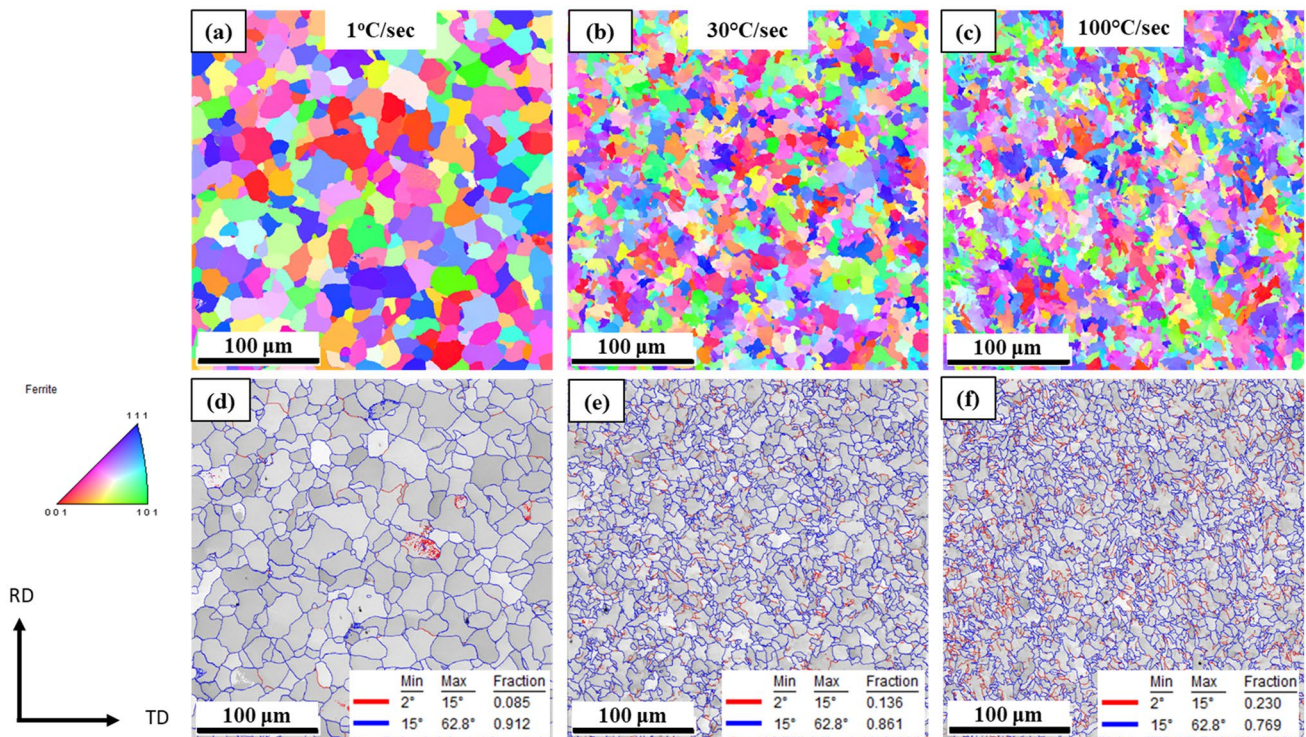
Fig. 11 **(a-c)** IPF maps and **(d-f)** corresponding grain boundary maps of specimens subjected to cooling rates of 1, 30 and 100°C/s, respectively

fibre accompanied by the replacement of *rotated cube*, viz. {100}<011> components by the *transformed copper*, viz. {112}<110>, {113}<110> and {223} <110> components as the dominant texture components.

The intensities of the components that make up the "α" and the "γ" fibres are plotted in Fig. 13a and b, respectively. It can be seen from Fig. 13a that the intensity of the *rotated cube* component decreases and that of the *transformed copper* components increases with an increase in cooling rate. Furthermore, there is a significant decrease in the intensity of the "γ" fibre with increase in cooling rate. The inferences drawn from the aforementioned observations based on ODFs and the corresponding texture intensity plots are:

i. The strong *rotated cube* components present in the specimens subjected to cooling rates of 1 and 30 °C/s trace their origin to the "γ" recrystallization texture, viz. {100}<001> [1–3]. This is to be expected as the austenitizing temperature employed in the present study is 1100 °C that is well above the "γ" recrystallization temperature.

ii. The presence of the "γ" fibre in the specimen cooled at 1 °C/s indicates occurrence of recrystallization of the transformed α [49–51]. The disintegration of the "γ" fibre with increase in cooling rate is a direct result of the lesser time available for recrystallization

of the transformed α at faster cooling rates of 30 and 100 °C/s.

iii. The increase in the intensities of the "α" fibre components at the expense of the *rotated cube* and "γ" fibre components with increase in cooling rate is also a result of faster transformation and lack of recrystallization of transformed α at higher cooling rates.

Although the aforementioned inferences do not strictly conform to the findings discussed in the literature, the present study shows the cooling rate to have significant effect on the evolved texture of Nb–Ti microalloyed steel.

Conclusions

The effect of cooling rate on phase transformation kinetics, microstructure and microtexture of Nb–Ti microalloyed steel was investigated, and the following conclusions are drawn from this study.

1. The fraction transformed plotted with respect to time was subjected to modified JMAK analysis to derive an equation describing the phase transformation kinetics in the steel under present study. The change in the growth controlling mechanism with respect to cooling rate could not be ascertained as it had little influence on the expo-
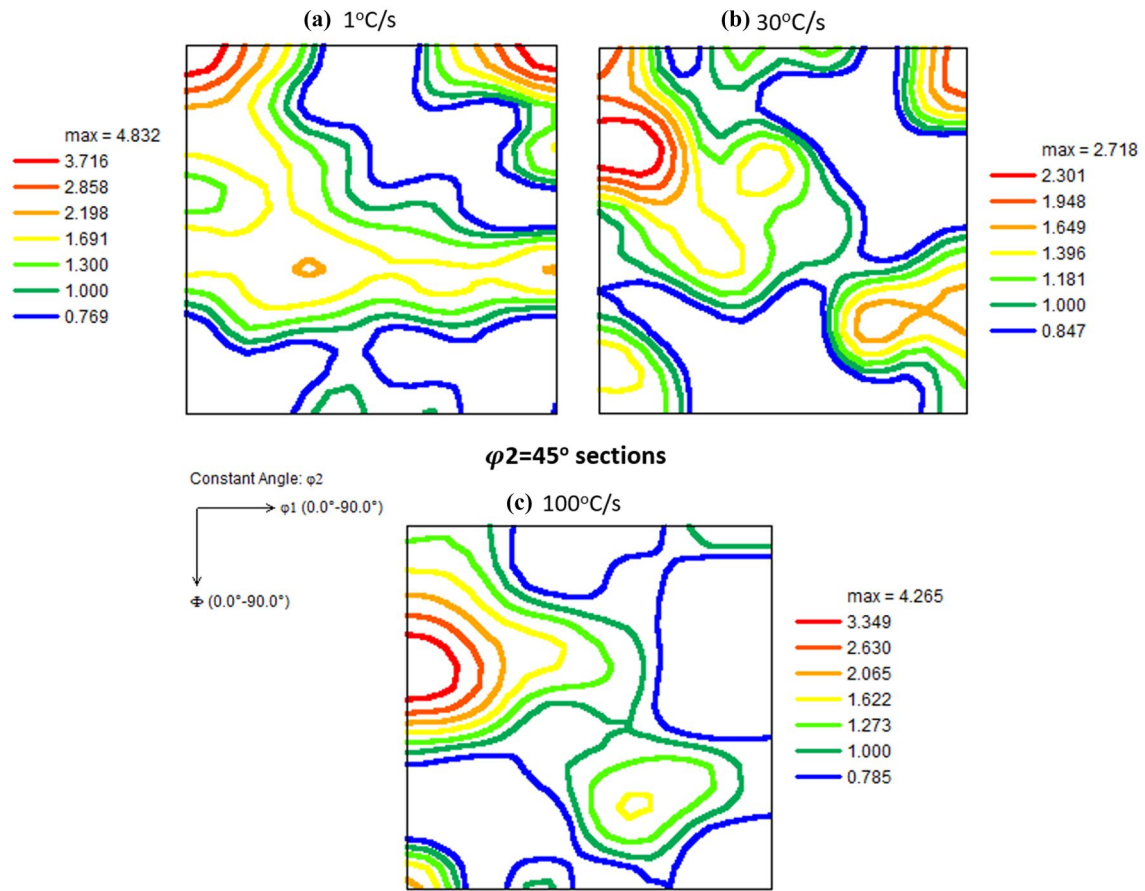
Fig. 12 ODF maps sectioned at φ_2 = 45 °C for the samples cooled with a cooling rate of **(a)** 1 °C/sec **(b)** 30 °C/sec and **(c)** 100 °C/sec
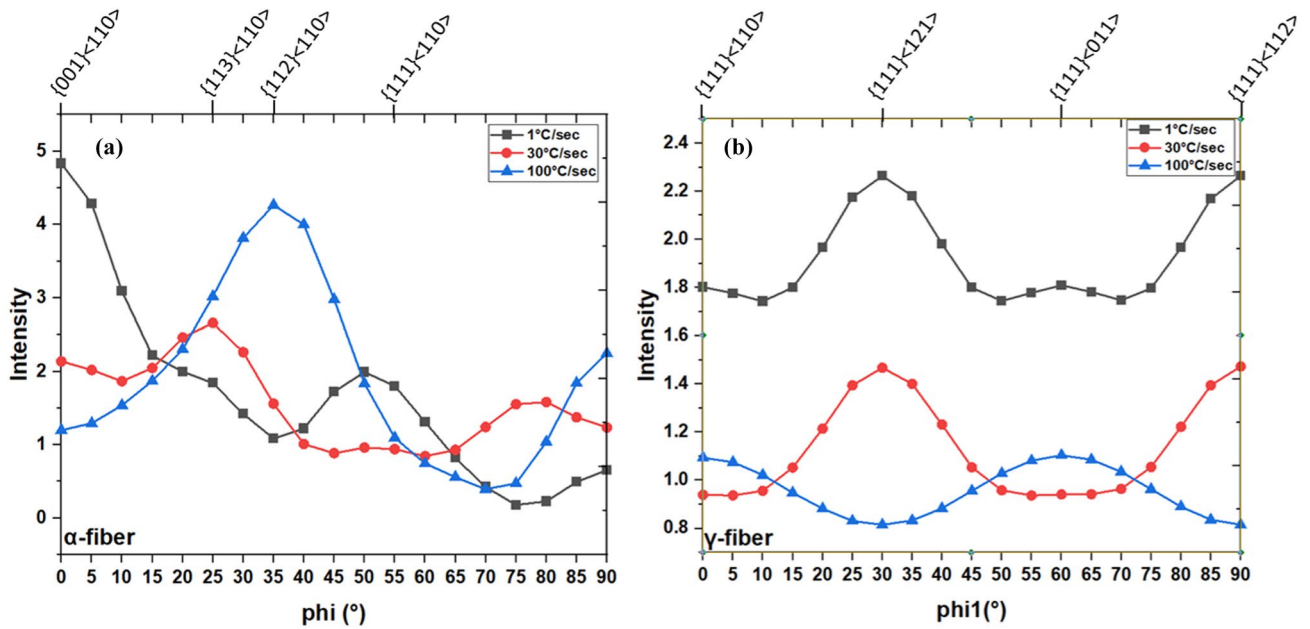

Fig. 13 Variation of intensity plots for the **(a)** α-fibre and **(b)** γ-fibre

nent (n'). However, a wide variation in the pre-exponent values ($t_{0.5}$) suggests that the activation energy for phase transformation is different at different cooling rates. Hence, from an industrial standpoint, choice of a cooling rate simply based on the exponent and pre-exponent values is not advised as both of them fail to provide any insight into the mechanism of phase transformation and the corresponding microstructural evolution.

2. The increase in cooling rate not only leads to a decrease in grain size but also changes the morphology of ferrite from polygonal to acicular. This indicates that at lower cooling rates, the growth is diffusion-controlled, whereas at higher cooling rates, it is interface controlled. Since, the mechanical properties vary with the ferrite morphology and grain size, the choice of cooling rate must be made based on the desired mechanical properties. This has been illustrated by establishing a power law and logarithmic relationship of grain size and microhardness with cooling rate, respectively.

3. The cooling rate significantly affects the texture evolution accompanying the phase transformation in Nb–Ti microalloyed steel. The "γ" fibre and rotated cube components are replaced by the transformed copper ("α" fibre) components owing to faster transformation and lack of recrystallization of transformed α with increase in cooling rate.

References

1. C.I. Garcia, Automotive Steels: Design, Metallurgy, Processing and Applications, in *High strength low alloyed (HSLA) steels*. ed. by R. Rana, S.B. Singh (Woodhead Publishing, Elsevier, 2017), pp. 145–168
2. T. Inoue, R. Ueji, Improvement of strength, toughness and ductility in ultrafine-grained low-carbon steel processed by warm bi-axial rolling. Mater. Sci. Eng. A. **786**, 139415 (2020)
3. F.B. Pickering, *Microalloying 75* (International Symposium on HSLA Steels, NY, 1975), pp. 9–15
4. T. Tanaka, In: International Conference on HSLA Steels. N.S.W: Wollongong; 6 1984
5. C.J. Crisbacher, J.H. Gross, R.D. Stout, J.J. Todaro, In: International Symposium on High Performance Steels for Structural Applications. Ohio: Clevland, 75 1995
6. C.I. Garcia, A.J. DeArdo, E. Raykin, J.D. Defilippi, In: international symposium on high performance steels for structural applications. Ohio: Clevland, 155 1995
7. S. Chatterjee, N.S. Misra, Evolution of acicular ferritic microstructure in a titanium bearing HSLA steel. Steel Res. Int. **65**, 138–145 (1994)
8. M.F. Mekkawy, K.A. El-Farwakhry, M.L. Mishreky, M.M. Eissa, Effect of interrupted accelerated cooling on mechanical properties and structure of vanadium and titanium microalloyed steel bars. Mater. Sci. Technol. **7**(1), 28–36 (1991)
9. A. Streibelberger, R. Kaspar, O. Pawelski, Improving mechanical properties of microalloy steels by modified thermomechanical treatments. Mater. Sci. Technol. **1**(2), 121–127 (1985)
10. Y. Hai-Long, D. Lin-Xiu, W. Guo-Dong, L. Xiang-Hua, Development of a hot-rolled low carbon steel with high yield strength. ISIJ Int. **46**(5), 754–758 (2006)
11. J. Fernández, S. Illescas, J.M. Guilemany, J.M., Effect of micro-alloying elements on the austenitic grain growth in a low carbon HSLA steel. Mater. Lett. **61**, 2389–2392 (2007)
12. A. Grajcar, S. Lesz, Influence of Nb microaddition on a microstructure of low-alloyed steels with increased manganese content. Mater. Sci. Forum. **706**, 2124–2129 (2012)
13. D.Q. Bai, S. Yue, T.M. Maccagno, J.J. Jonas, Effect of deformation and cooling rate on the microstructures of low carbon Nb-B steels. ISIJ Int. **38**, 371–379 (1998)
14. P. Palček, B. Hadzima, M. Chalupová, Experimental methods in engineering materials (in Slovak) Žilina, EDIS ŽU Žilina, ISBN 80-8070-179-2 2004
15. J. Calvo, I.H. Jung, A.M. Elwazri, D.Q. Bai, S. Yue, Influence of the chemical composition on transformation behaviour of low carbon microalloyed steels. Mater. Sci. Eng., A. **520**(1–2), 90–96 (2009)
16. P. Gong, E.J. Palmiere, W. Rainforth, Dissolution and precipitation behaviour in steels microalloyed with niobium during thermomechanical processing. Acta Mater. **97**, 392–403 (2015)
17. Y. Shu-Biao, S. Xin-Jun, L. Qing-You, Z. Zhi-Bo, Influence of deformation of low-carbon and high Nb-containing steel during continuous cooling. J. Iron. Steel Res. Int. **17**(2), 43–47 (2010)
18. M.C. Zhao, K. Yang, F. Xiao, Y. Shan, Continuous cooling transformation of undeformed and deformed low carbon pipeline steels. Mater. Sci. Eng., A. **355**(1–2), 126–136 (2003)
19. M.G. Mecozzi, J. Sietsma, S. Van der Zwaag, Analysis of $\gamma\rightarrow\alpha$ transformation in a Nb micro-alloyed C-Mn steel by phase field modelling. Acta Mater. **54**(5), 1431–1440 (2006)
20. M. Morawiec, A. Skowronek, M. Król, A. Grajcar, Dilatometric analysis of the austenite decomposition in undeformed and deformed low-carbon structural steel. Materials. **13**, 5443 (2020)
21. T.A. Kop, J. Sietsma, S. Van Der Zwaag, Dilatometric analysis of phase transformations in hypo-eutectoid steels. J. Mater. Sci. **36**, 519–526 (2001)
22. H. Boyer, *Atlas of isothermal transformation and cooling transformation diagrams* (Material Park, Ohio, 1977)
23. B.T. Alexandrov, J.C. Lippold, Single sensor differential thermal analysis of phase transformations and structural changes during welding and postweld heat treatment. Weld. World. **51**, 48–59 (2007)
24. M.I. Barrena, J.M.G.D. Salazar, L. Pascual, Determination of the kinetic parameters in magnesium alloy using TEM and DSC techniques[J]. J. Therm. Anal. Calorim. **113**(2), 713–720 (2013)
25. J.L. Béchade, D. Menut, S. Doriot, X-ray diffraction analysis of secondary phases in zirconium alloys before and after neutron irradiation at the MARS synchrotron radiation beamline. J. Nucl. Mater. **437**(1–3), 365–372 (2013)
26. O.N. Mohanty, A.N. Bhagat, Electrical resistivity and phase transformation in steels. Mater. Wiss. Und Werkst. **34**(1), 96–101 (2003)
27. Y.E. Smith, A.P. Coldren, R.L. Cryderman, Toward Improved Ductility and Toughness, Climax molybdenum company (Japan) Ltd, Tokyo, 119–142 1972
28. A. Ghosh, S. Das, S. Chatterjee, P. Ramachandra Rao, Effect of cooling rate on structure and properties of an ultra-low carbon HSLA-100 grade steel. Mater. Charact. **56**, 59–65 (2006)
29. R. Shukla, S.K. Ghosh, D. Chakrabarti, S. Chatterjee, Microstructure, texture, property relationship in thermo-mechanically

processed ultra-low carbon microalloyed steel for pipeline application. Mater. Sci. Eng. A. **587**, 201–208 (2013)

30. S. Kim, S.-H. Choi, S.-H. Kim, S.-J. Seo, I.S. Suh, Influence of micro-texture on delamination of hot-rolled high strength low alloyed steel sheets. HSLA Steels 2015, Microalloying 2015 & Offshore Engineering Steels 2015. Conference Proceedings. Springer International Publishing, 267–271 2016

31. L. Storojeva, D. Ponge, R. Kaspar, D. Raabe, Development of microstructure and texture of medium carbon steel during heavy warm deformation. Acta Mater. **52**, 2209–2220 (2004)

32. H.-T. Liu, H.-L. Li, J. Schneider, Y. Liu, G.D. Wang, Effects of coiling temperature after hot rolling on microstructure, texture, and magnetic properties of non-oriented electrical steel in strip casting processing route. Steel Res. Int. **87**, 1256–1263 (2016)

33. R. Song, D. Ponge, D. Raabe, R. Kaspar, Microstructure and crystallographic texture of an ultrafine grained C-Mn steel and their evolution during warm deformation and annealing. Acta Mater. **53**, 845–858 (2005)

34. N.M.L. Granados, A.S. Rodriguez, EBSD investigation on effect of cooling rate on microstructure and transformation textures of high strength hot rolled steel plate. J. Iron. Steel Res. Int. **23**(3), 261–269 (2016)

35. C.G. Andres, F.G. Caballero, C. Capdevila, D.S. Martin, Revealing austenite grain boundaries by thermal etching: advantages and disadvantages. Mater. Charact. **49**(2), 121–127 (2002)

36. B.J. Park, J.M. Choi, K.J. Lee, Analysis of phase transformations during continuous cooling by the first derivative of dilatation in low carbon steels. Mater. Charact. **64**, 8–14 (2012)

37. M. Takahashi, H.K.D.H. Bhadeshia, The interpretation of dilatometric data for transformations in steels. J. Mater. Sci. Lett. **8**, 477–478 (1989)

38. M. Onink, F.D. Tichelaar, C.M. Brakman, E.J. Mittemeijer, S. van der Swaag, Quantitative analysis of the dilatation by decomposition of Fe-C Austenites; calculation of volume change upon transformation. Zeitschrift Fur Metallkunde. **87**(1), 24–32 (1996)

39. T. A. Kop, Sietsma, J., Zwaag, S.: Proc. Materials Solutions '97 on Accelerated Cooling/Direct Quenching Steels, ASM International, Materials Park, OH, 159, (1997)

40. M. Avrami, Kinetics of phase change. I General Theory. J. Chem. Phys. **7**(12), 1103–1112 (1939)

41. M. Gómez, S.F. Medina, G. Caruana, Modelling of phase transformation kinetics by correction of dilatometry results for a ferritic nb-microalloyed steel. ISIJ Int. **43**(8), 1228–1237 (2003)

42. C.M. Sellars, The physical metallurgy of hot working, in *Hot Working and Forming Processes*. ed. by C.M. Sellars, G.J. Davies (The Metals Society, London, 1980), pp. 3–15

43. R.A. Cardosoa, G.L. Faria, Characterization of austenite decomposition in steels with different chemical concepts and high potential to manufacture seamed pipes for oil and gas industry. Mater. Res. (2019). https://doi.org/10.1590/1980-5373-mr-2019-0378

44. A.L.S. Cezárioa, G. Lúcio, de Fariaa, Proposition of an Empirical Functional Equation to Predict the Kinetics of Austenite to Ferrite Transformation in a Continuous Cooled IF-Ti-Stabilized Steel. Mater. Res. (2021). https://doi.org/10.1590/1980-5373-mr-2020-0498

45. Y.B. Guo, G.F. Sui, Y.C. Liu, Y. Chen, D.T. Zhang, Phase transformation mechanism of low carbon high strength low alloy steel upon continuous cooling. Mater. Res. Innov. **19**(sup8), 416–422 (2015)

46. S.B. Singh, K. Krishnan, S.S. Sahay, Modeling non-isothermal austenite to ferrite transformation in low carbon steels. Mater. Sci. Eng., A. **445–446**, 310–315 (2007)

47. M. Umemoto, Z.H. Guo, I. Tamura, Effect of cooling rate on grain size of ferrite in a carbon steel. Mater. Sci. Technol. **3**, 249–255 (1987)

48. A.A. Gorni, P.R. Mei, Austenite transformation and age hardening of HSLA-80 and ULCB steels. J. Mater. Process. Technol. **155–156**, 1513–1518 (2003)

49. J.J. Jonas, Transformation textures associated with steel processing, in *Microstructure and texture in steel*. ed. by A. Haldar, S. Suwas, D. Bhattacharjee (Springer, 2009), pp. 3–17

50. R.K. Ray, J.J. Jonas, Transformation textures in steels. Int. Mater. Rev. **35**, 1–36 (1990)

51. V. Javaheri, N. Khodaieb, A. Kaijalainen, D. Porter, Effect of niobium and phase transformation temperature on the microstructure and texture of a novel 040% C thermomechanically processed steel. Mater. Charact. **142**, 295–308 (2018)

52. M.C. Zhao, K. Yang, F.R. Xiao, Y.Y. Shan, Continuous cooling transformation of undeformed and deformed low carbon pipeline steels. Mater. Sci. Eng. A. **355**, 126–136 (2003)